Two vertical bars are positioned on the left side of the page: a thick blue bar and a thinner cyan bar, both extending from the top to the bottom of the page.

**NORSAR Scientific Report No. 2-2012**

**Semiannual Technical Summary**

**1 July – 31 December 2012**

**Tormod Kværna (Ed.)**

**Kjeller, June 2013**

---

## 6.2 Automatic Parameter Extraction for Three-Component Observations

### 6.2.1 Introduction

The development of data processing software at NORSAR concentrated during the last decades on reliable results for an automatic analysis of array data. NORSAR's system of STA/LTA detectors on different filtered data streams can easily be copied to the case of a single 3-component (3C) station, just without involving any beamforming of data from different array sites. However, any further data analysis and parameter extraction cannot be adapted so easily to an automatic analysis of 3C data. Although an analyst will recognize in most cases just by visual inspection the type of a seismic onset (P or S or surface phase), an automated analysis tool will encounter problems. The challenge in any 3C data analysis is reliable phase type identification, and without any possibility to measure the later parameters with an array, *e.g.*, by *fk*-analysis, the estimation of backazimuth (BAZ) and incidence angle (INC). INC is related to the apparent velocity, as measured with an array, via Snell's law.

Observations of seismic phases do not obviously show their character at first face: P- as well as S-phases are usually recorded with adequate amplitudes on all components of a 3C station. The analysis of the particle motion (polarization analysis) should solve the problem because the seismic phases can be separated after rotating the 3C traces of the station (ZNE) into a ray oriented Cartesian coordinate system (LQT): *e.g.*, pure P-phases should be only visible on the Longitudinal-trace (L-component), pure S-phases should be only visible on the two perpendicular oriented coordinates Q- (for SV-energy) and T- (for SH-energy), and the surface phase Rg should only have energy on the L- and Q-components.

However, real data are rarely pure onsets because P-to-SV and SV-to-P conversions occur at discontinuities and lateral heterogeneities. In addition, coda energy caused by the scattering of seismic waves, can be observed for all onsets, and may arrive at the observing station even from different BAZ directions than the main phase. Thus, seismic onsets are mixtures of the main phase and all these different types of disturbances, plus the time depending background noise. This makes polarization analysis of seismic phases more difficult, complicates its interpretation and contributes to the known scatter of polarization results.

In this contribution, a strategy and its theoretical background are presented on how the uncertainties of 3C data analysis results can be reduced and more reliable BAZ and apparent velocity parameters can be estimated, by applying an analysis algorithm consisting of several steps.

### 6.2.2 The approach

Assuming that the observed onset is either a P-, or an Rg- or an S-onset, one can separate the analysis in four steps:

- At first, the 3C data are rotated in the LQT-coordinate system under the assumption that the onset is a P-phase. If the phase under investigation is really a P-phase, BAZ and INC values must exist for which all energy is concentrated on the L component, while the Q- and T-components are almost zero. But *e.g.*, also an almost horizontally propagating, vertically polarized S-onset will have large vertical amplitudes but small horizontal amplitudes and can therefore be misinterpreted as a P-phase.

- In a second step, the Rg-phase hypothesis is assumed. For Rg-phases, one expects only energy on the L- and Q-components, with slightly larger amplitudes on the Q-component. The T-component should be zero as for P-type onsets.
- The third step is an analysis under the assumption that the onset is an S-phase. In this case, it should be possible to rotate the 3C data for one BAZ and INC value so, that in the L, Q, T system the L component has zero amplitudes and all the energy is concentrated on the Q and T components.
- In a last step, the results found for the different phase types, BAZ and INC combinations are compared and weighted to decide if the observed phase is most probably a P-, an Rg- or an S-phase and which BAZ and incidence angle (*i.e.*, slowness) fits best with this phase identification.

In any case, this approach is based on the assumption that there is only one dominating seismic phase type, which reaches the station from below. Seismic signals coming from above the 3C station (as *e.g.*, recordings by underground installations or of acoustic signals) cannot be correctly analyzed.

### 6.2.3 The method

At first some basic formulas and definitions are listed:

Z	vertical component of the 3C recording
E	east-west oriented horizontal component of the 3C recording
N	north-south oriented horizontal component of the 3C recording
R	radial component after rotating the horizontal components for a specific BAZ
T	transverse component after rotating the horizontal components for a specific BAZ; identical with the SH component after rotating all three components in the ray oriented LQT-coordinate system by applying a specific BAZ and INC
Q	SV component after rotating all three components in the ray oriented LQT-coordinate system by applying a specific BAZ and INC
L	longitudinal = compressional P-component after rotating all three components in the ray oriented LQT-coordinate system by applying a specific BAZ and INC
BAZ	backazimuth, angle $\varphi$ measured between North and the direction of the incoming wavefield (onset) at the seismic station
INC	incidence angle $\alpha$ measured between the horizontal plane and the direction of the incoming wavefield (onset) at the seismic station

The relation between the different components is defined as:

$$R = -N * \cos(BAZ) - E * \sin(BAZ)$$

$$T = +N * \sin(BAZ) - E * \cos(BAZ)$$

$$L = +Z * \cos(INC) + R * \sin(INC)$$

$$Q = -Z * \sin(INC) + R * \cos(INC)$$

Squaring these formulas gives:

$$\begin{aligned}
 R^2 &= N^2 * \cos^2(BAZ) + 2NE * \cos(BAZ) * \sin(BAZ) + E^2 * \sin^2(BAZ) \\
 T^2 &= N^2 * \sin^2(BAZ) - 2NE * \cos(BAZ) * \sin(BAZ) + E^2 * \cos^2(BAZ) \\
 L^2 &= Z^2 * \cos^2(INC) + 2ZR * \cos(INC) * \sin(INC) + R^2 * \sin^2(INC) \\
 Q^2 &= Z^2 * \sin^2(INC) - 2ZR * \cos(INC) * \sin(INC) + R^2 * \cos^2(INC)
 \end{aligned}$$

#### 6.2.4 P-phase inversion

To invert for the best BAZ and INC in the case of a P-phase, the Q- and T-components have to be minimized, which means that

$$\begin{aligned}
 Q &= 0; T = 0; L = \sqrt{N^2 + E^2 + Z^2}; R = \sqrt{N^2 + E^2} \\
 Q^2 &= 0; T^2 = 0; L^2 = N^2 + E^2 + Z^2; R^2 = N^2 + E^2
 \end{aligned}$$

First, the BAZ is estimated by solving with a Least-Squares algorithm (LSQ) the following system of n+1 equations

$$\begin{bmatrix} N_1^2 & -2N_1E_1 & E_1^2 \\ \vdots & \vdots & \vdots \\ N_n^2 & -2N_nE_n & E_n^2 \\ 1 & 0 & 1 \end{bmatrix} * \begin{bmatrix} \sin^2(BAZ) \\ \sin(BAZ) * \cos(BAZ) \\ \cos^2(BAZ) \end{bmatrix} = \begin{bmatrix} 0 \\ \vdots \\ 0 \\ 1 \end{bmatrix}, \quad (\text{Eq. 1})$$

for the n samples in the time window that has to be analyzed. The three unknown variables are  $\sin^2(BAZ)$ ,  $\sin(BAZ) * \cos(BAZ)$  and  $\cos^2(BAZ)$ . The last, (n+1)<sup>th</sup> equation is a side condition to avoid a zero solution and to force that  $\sin^2(BAZ) + \cos^2(BAZ) \equiv 1$ . Then, the backazimuth  $\varphi$  is defined as

$$\varphi = \text{atan}\sqrt{\sin^2(BAZ)/\cos^2(BAZ)} \quad (\text{Eq. 2})$$

Because of the periodicity of the trigonometric functions, one gets four different solutions:

$$BAZ = \left\{ 180 + \varphi \right\} \text{ if } \sin(BAZ) * \cos(BAZ) \geq 0 \quad (\text{Eq. 3})$$

$$BAZ = \left\{ 180 - \varphi \right\} \text{ if } \sin(BAZ) * \cos(BAZ) < 0 \quad (\text{Eq. 4})$$

Theoretically, the sign of the inverted parameter  $\sin(BAZ) * \cos(BAZ)$  is reducing the four into two possible solutions. However, for BAZ values close to the original coordinate axes and higher noise levels, the application of this rule may lead to wrong results at this stage. Using only horizontal components, the ambiguity between the two remaining possibilities cannot be resolved. Therefore, all four possible BAZ values are considered in the following analysis steps.

The LSQ algorithm gives also standard deviations ( $\sigma_{\sin^2(BAZ)}, \sigma_{\cos^2(BAZ)}$ ) for the unknown variables of Eq. 1. These standard deviations  $\sigma_{BAZ}$  can then be used to calculate the uncertainty of the BAZ estimates by applying standard rules for calculating derivatives and Gauss' law of error propagation:

$$\sigma_\varphi = \sqrt{\frac{\partial\varphi}{\partial\sin^2(BAZ)} * \sigma_{\sin^2(BAZ)}^2 + \frac{\partial\varphi}{\partial\cos^2(BAZ)} * \sigma_{\cos^2(BAZ)}^2} = \frac{1}{2} * \sqrt{\cot^2(BAZ) * \sigma_{\sin^2(BAZ)}^2 + \tan^2(BAZ) * \sigma_{\cos^2(BAZ)}^2} \quad (\text{Eq. 5})$$

To invert also for the incidence angle  $\alpha$ , a second equation system has to be solved under the condition that the energy on the Q-component should also become minimum when applying the four possible BAZ values to calculate R:

$$\begin{bmatrix} Z_1^2 & -2Z_1R_1 & R_1^2 \\ \vdots & \vdots & \vdots \\ Z_n^2 & -2Z_nR_n & R_n^2 \\ 1 & 0 & 1 \end{bmatrix} * \begin{bmatrix} \sin^2(INC) \\ \sin(INC) * \cos(INC) \\ \cos^2(INC) \end{bmatrix} = \begin{bmatrix} 0 \\ \vdots \\ 0 \\ 1 \end{bmatrix}, \quad (\text{Eq. 6})$$

As shown for Eq.1, Eq. 6 can be solved for the unknown variables  $\sin^2(INC)$ ,  $\sin(INC) * \cos(INC)$  and  $\cos^2(INC)$ . The incidence angle  $\alpha$  is then defined as:

$$\alpha = \text{atan}\sqrt{\sin^2(INC)/\cos^2(INC)} \quad (\text{Eq. 7})$$

The standard deviation  $\sigma_\alpha$  can then be derived in analogy to  $\sigma_{BAZ}$ :

$$\sigma_\alpha = \sqrt{\frac{\partial\alpha}{\partial\sin^2(INC)} * \sigma_{\sin^2(INC)}^2 + \frac{\partial\alpha}{\partial\cos^2(INC)} * \sigma_{\cos^2(INC)}^2} = \frac{1}{2} * \sqrt{\cot^2(INC) * \sigma_{\sin^2(INC)}^2 + \tan^2(INC) * \sigma_{\cos^2(INC)}^2} \quad (\text{Eq. 8})$$

There is a trade-off between the sign of  $\sin(INC) * \cos(INC)$  and the incidence direction of the seismic phase. At this stage, one has to make the assumption that the seismic phase is reaching the station either from below or above the seismic station. In the algorithm described herein, the assumption is made that seismic waves are coming from below in the case of body waves or horizontally in the case of surface waves. Then, a negative sign of  $\sin(INC) * \cos(INC)$  indicates that the phase arrives from the opposite direction (a 180° change) than the applied BAZ, which theoretically solves the 180° ambiguity of Eqs. 3 and 4.

It is well known that seismic stations at the Earth's surface record a mixture of directly arriving and reflected seismic energy. The reflected wavefield can contain P-to-S or S-to-P converted waves, which changes the amplitude ratio between the vertical and horizontal components in a characteristic way and consequently influences the measured incidence angle  $\alpha$ , which is therefore called an apparent incidence angle. Following Wiechert (1907) or *e.g.*, Müller (2007), for P-phases the relation between the apparent incidence angle  $\alpha$  and the free-surface corrected incidence angle  $\beta$  can be written as

$$\alpha = \arctan\left(\frac{2 * \sin(\beta) * (\gamma - \sin^2(\beta))^{1/2}}{(\gamma - 2 * \sin^2(\beta))}\right).$$

Knowing the seismic velocity ratio  $\gamma = (v_p/v_s)^2$  below the 3C station and assuming that  $\alpha$  is always positive and  $v_p$  is always larger than  $v_s$ , one can show that

$$\sin^2(\beta) = \frac{\gamma}{2}(1 - \cos(\alpha))$$

and

$$\beta = \arcsin\left(\frac{v_P}{v_S} * \sin\left(\frac{\alpha}{2}\right)\right). \quad (\text{Eq. 9})$$

The uncertainty of  $\beta$  is then

$$\sigma_\beta = (\partial\beta/\delta\alpha) * \sigma_\alpha = \frac{v_P}{2*v_S} * \frac{\cos(\alpha/2)}{\cos(\beta)} * \sigma_\alpha \quad (\text{Eq. 10})$$

By knowing the local P velocity one can also convert the apparent or the free-surface corrected incidence angles into apparent velocities by applying Snell's law

$$v_{app} = \frac{v_P}{\sin(inc)} \quad (\text{Eq. 11})$$

with an uncertainty of

$$\sigma_{vapp} = v_{app} * \tan(inc) * \sigma_{inc} \quad (\text{Eq. 12})$$

The corrected incidence angle and the apparent velocity including their uncertainties depend on the seismic velocities below the station. In the real Earth, where seismic velocities change with depth, the velocities to be used are the effective velocities of the uppermost layers, depending on the dominant wavelength of the analyzed seismic phase. Contrary to measurements with a seismic array without topography effects (see *e.g.*, Schweitzer *et al.*, 2012), in the 3C case all incidence angle and apparent velocity measurements become frequency depending.

### 6.2.5 Rg-phase inversion

Rg-phases can be handled as part of the P-phase case. Eqs. 1 – 2 are also true for Rg-onsets: The best BAZ for Rg-phases minimizes the energy on the T-component. However, Rg-phases have significant energy on the Z- and R-components. In addition, contrary to P type onsets, one can observe a time shift between the Rg-onsets on the Z- and R-components. Therefore, it does not make sense to rotate this phase in an LQT-coordinate system. To test this, R-traces are calculated for all four possible BAZ values and then cross-correlated with the original Z-component. Another possibility would be to compare the two traces after a Hilbert transform of one of them. Whenever a significant time shift between the onsets on both components is observed, this is taken as a strong indication for an Rg-onset, since such time shifts are not observable for P or S-phases.

### 6.2.6 S-phase inversion

In the case of an S-phase, one can only use the rule that in the LQT-system the L-component should show no energy, all seismic energy being polarized in a plane perpendicular to the propagation direction. The distribution of energy between the Q- and T-components mostly depends on the radiation pattern of SV and SH at the seismic source and cannot be used here as an analysis criterion.

In a first step, the best fitting BAZ and INC are inverted for, to minimize the L-component. Once again some definitions:

$$U \equiv N^2 + E^2 + Z^2 \equiv T^2 + Q^2 \quad (\text{Eq. 13})$$

From  $L = +Z * \cos(INC) + R * \sin(INC) = 0$  follows that  $Z = -R * \tan(INC)$  and  $R = -Z * \tan(INC)$ . Using these relations and  $Q^2 = R^2 + Z^2$  one can show that

$$Q^2 = Z^2 * \frac{1}{\sin^2(INC)}. \quad (\text{Eq. 14})$$

Setting the definition of  $T^2 = N^2 * \sin^2(BAZ) + 2NE * \cos(BAZ) * \sin(BAZ) + E^2 * \cos^2(BAZ)$  and of  $Q^2$  from Eq. 14 in Eq. 13 one gets:

$$N^2 * \sin^2(BAZ) - 2NE * \cos(BAZ) * \sin(BAZ) + E^2 * \cos^2(BAZ) + \frac{Z^2}{\sin^2(INC)} = U$$

$$\frac{N^2 * \sin^2(BAZ)}{U} - \frac{2NE * \cos(BAZ) * \sin(BAZ)}{U} + \frac{E^2 * \cos^2(BAZ)}{U} + \frac{Z^2}{U * \sin^2(INC)} = 1$$

This can be solved again with the LSQ algorithm as in the P-phase case, with the only difference that there are now four unknowns:

$$\begin{bmatrix} \frac{N_1^2}{U} & \frac{-2N_1E_1}{U} & \frac{E_1^2}{U} & \frac{Z_1^2}{U} \\ \vdots & \vdots & \vdots & \vdots \\ \frac{N_n^2}{U} & \frac{-2N_nE_n}{U} & \frac{E_n^2}{U} & \frac{Z_n^2}{U} \\ 1 & 0 & 1 & 0 \end{bmatrix} * \begin{bmatrix} \sin^2(BAZ) \\ \sin(BAZ) * \cos(BAZ) \\ \cos^2(BAZ) \\ 1/\sin^2(INC) \end{bmatrix} = \begin{bmatrix} 1 \\ \vdots \\ 1 \\ 1 \end{bmatrix}, \quad (\text{Eq. 15})$$

As for the P-phase case, the backazimuth  $\varphi$  can be determined by applying Eq. 2 and for its uncertainty  $\sigma_\varphi$  Eq. 5 can be used:

$$\varphi = \text{atan} \sqrt{\sin^2(BAZ) / \cos^2(BAZ)} \quad (\text{Eq. 15})$$

$$\sigma_\varphi = \frac{1}{2} * \sqrt{\cot^2(BAZ) * \sigma_{\sin^2(BAZ)}^2 + \tan^2(BAZ) * \sigma_{\cos^2(BAZ)}^2} \quad (\text{Eq. 16})$$

With the fourth modeled parameter  $a = 1/\sin^2(INC)$  the incidence angle  $\alpha$  can be calculated:

$$\alpha = \arcsin \left( \sqrt{\frac{1}{a}} \right), \quad (\text{Eq. 17})$$

and the uncertainty  $\sigma_\alpha$  is defined as

$$\sigma_\alpha = \frac{\partial \alpha}{\partial a} * \sigma_{1/\sin^2(INC)} = \frac{1}{2a} * \tan(\alpha) * \sigma_{1/\sin^2(INC)} \quad (\text{Eq. 18})$$

To obtain the apparent velocity of the S-onset one has to apply again Snell's law, now with the local S velocity  $v_S$  as input parameter:

$$v_{app} = \frac{v_S}{\sin(INC)} \quad (\text{Eq. 19})$$

The uncertainty of the apparent S-velocity becomes

$$\sigma_{vapp} = v_{app} * \tan(\alpha) * \sigma_{\alpha}. \quad (\text{Eq.20})$$

The S-phase incidence angle is also influenced by the free-surface effect, but contrary to the case of P-phases there exists no uniform theoretical solution to correct for this. Therefore, incidence angles of S-phases and consequently their apparent velocities are not identical with other measuring methods like *e.g.*, array-based fk-results.

Also for S-phases exists the ambiguity between the different BAZ values due to the properties of the trigonometric functions. This problem can only be solved in a later stage. Tests made for numerous examples showed that inverting for both parameters (BAZ and INC) in one step does not always give the best solution. Therefore, two additional inversions are added to validate the found results.

- 1) At first the obtained BAZ values are used to calculate T- and R-traces and then an inversion is performed to find the best INC values. This is done in analogy to Eq. 6, but now for a minimized L-component:

$$\begin{bmatrix} R_1^2 & 2R_1Z_1 & Z_1^2 \\ \vdots & \vdots & \vdots \\ R_n^2 & 2R_nZ_n & Z_n^2 \\ 1 & 0 & 1 \end{bmatrix} * \begin{bmatrix} \sin^2(INC) \\ \sin(INC) * \cos(INC) \\ \cos^2(INC) \end{bmatrix} = \begin{bmatrix} 0 \\ \vdots \\ 0 \\ 1 \end{bmatrix}, \quad (\text{Eq. 21})$$

The incidence angle  $\alpha$  can then again be calculated with Eq. 7 and its uncertainty with Eq. 8. For obtaining the corresponding apparent velocities and their uncertainties one can apply Eqs. 19 and 20.

- 2) Then, in a second additional inversion the obtained INC value from Eq. 17 is applied and the corresponding best BAZ values are calculated:

When setting  $R = -Z / \tan(INC)$  in the definition of the  $R^2$  one gets

$$R^2 = E^2 * \sin^2(BAZ) + 2NE * \cos(BAZ) * \sin(BAZ) + N^2 * \cos^2(BAZ) = \frac{Z^2}{\tan^2(INC)}$$

and one can define the equation system:

$$\begin{bmatrix} \frac{E_1^2 * \tan^2(INC)}{Z^2} & \frac{2E_1N_1 * \tan^2(INC)}{Z^2} & \frac{N_1^2 * \tan^2(INC)}{Z^2} \\ \vdots & \vdots & \vdots \\ \frac{E_n^2 * \tan^2(INC)}{Z^2} & \frac{2E_nN_n * \tan^2(INC)}{Z^2} & \frac{N_n^2 * \tan^2(INC)}{Z^2} \\ 1 & 0 & 1 \end{bmatrix} * \begin{bmatrix} \sin^2(BAZ) \\ \sin(BAZ) * \cos(BAZ) \\ \cos^2(BAZ) \end{bmatrix} = \begin{bmatrix} 1 \\ \vdots \\ 1 \\ 1 \end{bmatrix}, \quad (\text{Eq. 22})$$

For solutions of the BAZ values  $\varphi$  one can again use Eq. 2 and for their uncertainties  $\sigma_{\varphi}$  Eq. 5. The results are all four new possible BAZ values because of the known ambiguity of the trigonometric functions.

## 6.2.7 Evaluation of the solutions and selection of the best possible phase estimate

The final step in this analysis scheme for seismic onsets observed with 3C stations is an evaluation of the different solutions and deciding on the most probable phase type, BAZ and INC (*i.e.*, apparent velocity) of the observation. This is done in two steps. In a first step, the best solution for each phase type is selected and in a second step, the results for three possible phase types are compared with

each other. To evaluate the different solutions, the original 3C traces are rotated into R-, T-, L- and Q-traces. Then, for each component C (*i.e.*, for Z, N, E, R, T, L and Q) the vector sums  $sZ$ ,  $sN$ ,  $sE$ ,  $sR$ ,  $sT$ ,  $sL$  and  $sQ$  are calculated over all samples  $i$  by using the formula  $sC = \sqrt{\sum_i sample_i^2}$ . In addition, normalized relations between some of the components ( $C_1C_2$ ) are calculated (*i.e.*, for RZ, RL, QZ, QR and ZL). For each of the relations between two components, the following formula is used

$$C_1C_2 = \frac{\sum_i sample_{c1} * sample_{c2}}{sC_1 * sC_2}.$$

Also the following sums are used during the different evaluation steps:

$$\begin{aligned} sH &= \sqrt{sQ^2 + sT^2}; \quad sH0 = \sqrt{sE^2 + sN^2} \equiv \sqrt{sT^2 + sR^2}; \\ SUM &= \sqrt{sZ^2 + sN^2 + sE^2}; \quad sRG = \sqrt{sZ^2 + sR^2}; \quad QT = sH/sH0 \end{aligned}$$

All these values are used to express phase type specific characteristics, as specified in the next sections. However, the applied relations are strictly true only for ideal onsets. In the following decisions the assumption is that the joint application of many different phase type specific characteristics will give the most plausible analysis result.

#### 6.2.7.1 The best P-phase solution

Assuming the phase is a P-phase, eight different solutions were found: four solutions for the BAZ and for each BAZ value one solution for an INC. For observed amplitudes on the different traces, an ideal P-phase should show the following relations between the above calculated parameters:

$$\begin{aligned} sL > sZ; \quad sL > sQ; \quad sL > sT; \quad sL > sH; \quad sL > sH0; \\ sR > sT; \quad sR > sQ; \quad sH0 > sH; \quad sL = SUM; \quad \text{and } RZ > 0 \end{aligned}$$

Taking these rules in a product of factors one can calculate the following decision factor:

$$F_p = \left| RZ * ZL * RL * \frac{RZ * sL * sL * sL * sR * sR * sL * sL * sH0}{QZ * sZ * sQ * sT * sT * sQ * sH0 * sH * sH} \right| = \left| \frac{RZ^2 * ZL * RL * sL^5 * sR^2}{QZ * sZ * sQ^2 * sT^2 * sH^2} \right| \quad (\text{Eq. 23})$$

All BAZ/INC combinations for which  $RZ < 0$  &  $sH > 0.2 * sL$  or  $sH > 1.05 * sH0$  or  $sL < 0.95 * sZ$  or  $sT > sR$  &  $sH0 > 0.2 * sL$  are directly rejected. Then, the P-phase with the largest value of  $F_p$  defines the most probable BAZ and INC.

#### 6.2.7.2 The best Rg-phase solution

The possible Rg-phase has four possible BAZ solutions. Being a surface wave, Rg has no values for INC, *i.e.*, the rotation from Z- and R- into Q- and L-components does not make any sense. However, time shifts found between the R- and the Z-components after the rotation of the original horizontal N- and E-components into R- and T-components are taken in account when calculating the above mentioned vector sums and trace relations. The following rules can be used to find the best parameters of the Rg-onset:

$$sZ > sT; \quad sR > sT; \quad sRG > sT; \quad sH0 > sT; \quad sRG > sZ; \quad sRG > sR; \quad \text{and } RZ > 0$$

Taking these rules as in a product of factors one can calculate the following decision factor:

$$F_{Rg} = \left| \frac{RZ*sR*sZ*sRG*sH0*sRG*sRG}{sT*sT*sT*sT*sZ*sR} \right| = \left| \frac{RZ*sRG^3*sH0}{sT^4} \right| \quad (\text{Eq. 24})$$

All solutions for which  $RZ < -0.1$  or  $sT > sZ$  or  $sT > sR$  are rejected. Then the parameters for BAZ and INC are chosen, which result in the largest value of  $F_{Rg}$ .

### 6.2.7.3 The best S-phase solution

From the three inversions for S-phases described in Section 6.2.6, one gets 12 different BAZ/INC combinations: four different BAZ values and one INC value from the first inversion, four different INC values from the second solution and four different BAZ values from the last inversion. The S-phase related rules are as following:

$$RQ > RZ; \quad sH > sH0; \quad sH > sZ; \quad sH > sL; \quad sH > sR; \quad sH > sT; \quad sH0 > sZ; \quad sZ > sL; \quad \text{and} \quad RZ < 0$$

Then one can define the following decision factor  $F_S$  for choosing the best S-phase onset:

$$F_S = \left| \frac{RQ*sH*sH*sH*sH*sH*sH0*sZ}{RZ*sH0*sZ*sL*sR*sT*sZ*sL} \right| = \left| \frac{RQ*sH^5}{RZ*sL^2*sR*sT*sZ} \right| \quad (\text{Eq. 25})$$

All combinations for which  $RZ > 0.5$  or  $sL > 1.05*sZ$  &  $sZ > 0.3*sH0$  or  $sH < 0.95*sH0$  are directly rejected. Then the parameters for BAZ and INC are chosen, which result in the largest value of  $F_S$ .

### 6.2.7.4 Choosing the right phase

To decide which one of the three phase types is the most likely one, a parameter  $D$  is calculated which is representative of the seismic energy of the different phase types. To avoid results biased by the chosen contributing factors, it is important that the parameter  $D$  consists for all three phase types of the same number of single factors with similar value ranges.

The parameters  $D$  are defined for the different phases as:

$$D_P = \left| \frac{ZL_P}{QT_P} \right| * \frac{sZ^3*sL_P^{15}}{sN^2*sE^2*sH_P*sH0_P*sQ_P^2*sT_P^2*sRG_P*sL_S*sL_{Rg}*sH_S*sH_{Rg}*sRG_S*sRG_{Rg}*SUM} \quad (\text{Eq. 26})$$

$$D_S = \left| \frac{QT_S}{ZL_S} \right| * \frac{sH0^3*sH_S^{15}}{sZ^2*sN*sE*sL_S^2*sQ_S^2*sT_S^2*sRG_S*sL_P*sL_{Rg}*sH_P*sH_{Rg}*sRG_P*sRG_{Rg}*SUM} \quad (\text{Eq. 27})$$

$$D_{Rg} = \left| \frac{RZ_{Rg}}{sT_{Rg}} \right| * \frac{sZ^2*sR_{Rg}^3*sRG_{Rg}^{13}}{sN^3*sE^3*sT_{Rg}^3*sH0^2*sL_P*sL_S*sH_P*sH_S*sRG_P*sRG_S*SUM} \quad (\text{Eq. 28})$$

Then, the phase type with the largest value of  $D$  is assumed to fit best with the observed onset and is chosen as the result of the 3C onset analysis.

## 6.2.8 Examples

From the formulas derived above it becomes clear that to decide on the phase type and best onset parameters BAZ and INC, the signal amplitudes should be clearly visible above the background noise level. In particular for components with theoretically small amplitudes, a relatively high noise level can easily result in wrong analysis results. In the following, some examples are shown for unequally successful analysis results and phase types. In all cases the algorithm decided about the phase type

by applying Eqs. 26 – 28 and reported the best fitting BAZ and INC values by applying Eqs. 23 – 25.

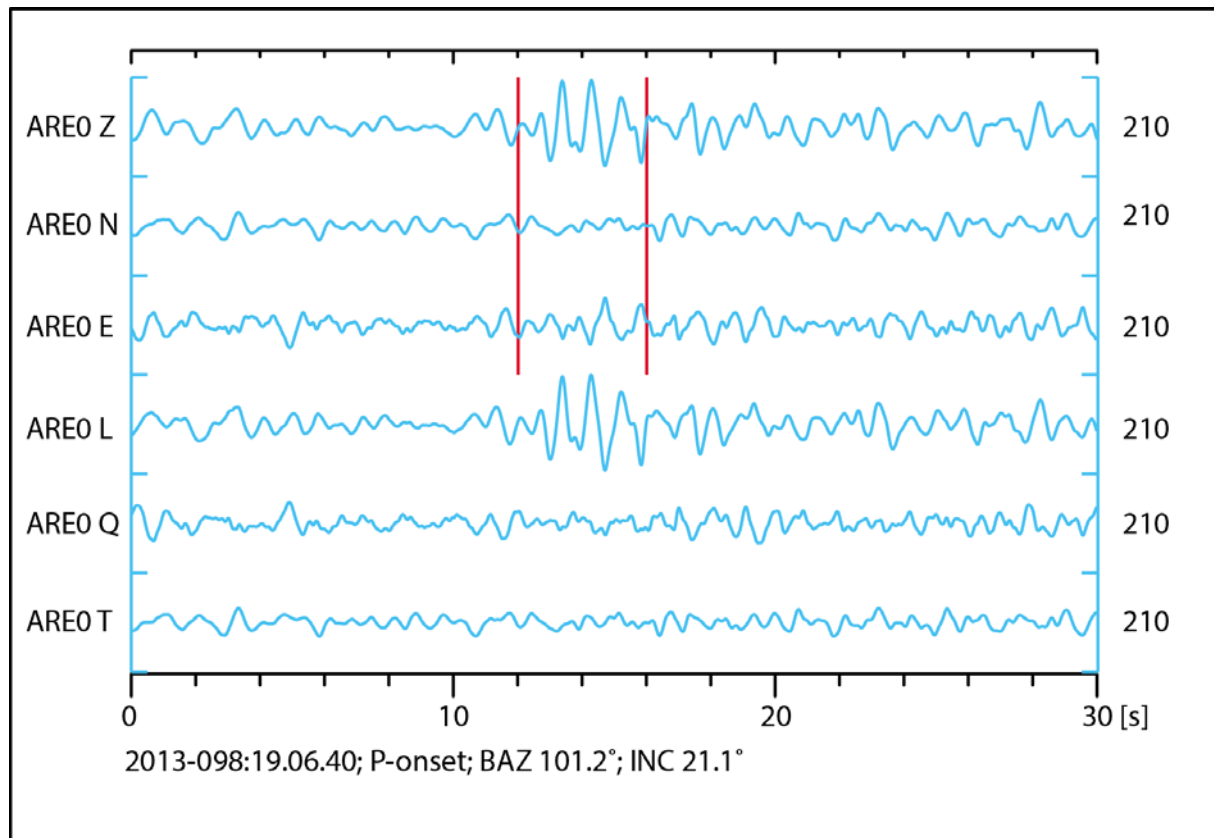


Fig. 6.2.1 Data (bandpass filtered 1 – 4 Hz) of a teleseismic P-onset observed at the ARCES 3C-site AREO. The time window used for the 3C analysis is marked (red lines) and the maximum amplitude is given on the right. The three top traces show the original 3C (ZNE) and the three bottom traces the LQT-rotated data. For further details see text.

Fig. 6.2.1 shows the P-onset of an mb 5.2 event (IDC REB hypocenter: Lat  $-6.99^\circ$ , Lon  $106.15^\circ$ , depth 47 km, source time 8 April 2013, 18:53:44) recorded with the 3C broadband station of the ARCES array (AREO) at a distance of  $93.24^\circ$ . The maximum signal-to-noise ratio (SNR) on the Z-component is 5.65, on E 2.60 and on the N-component only 1.84. The data are bandpass filtered for the best SNR between 1 and 4 Hz. The 3C analysis of the onset gave BAZ =  $81.54^\circ$  and INC =  $21.1^\circ$ , which, after applying the free surface correction, corresponds to an apparent velocity of 17.3 km/s. The theoretical values based on the REB location are BAZ =  $101.18^\circ$  and 24 km/s for the apparent velocity. The ARCES array analysis of all vertical components for the same time window gives BAZ =  $97.10^\circ$  and 22.5 km/s for the apparent velocity, which is much closer to the theoretically expected values. The discrepancies between theory and 3C analysis results are probably influenced by the low SNR values on the two horizontal components.

Fig. 6.2.2 shows the AREO recordings of a mining event at Kiruna (13 April 2013, 23:49:50). The applied bandpass filter was between 1.5 and 4.0 Hz and the 3C analysis tool was used for the clearly visible Sg-onset. The 3C analysis result was BAZ =  $214.9^\circ$  and INC =  $62.9^\circ$ , corresponding to an apparent velocity of 3.6 km/s. This fits with the theoretical values BAZ =  $231.2^\circ$  and an apparent velocity of 3.9 km/s. An fk-analysis of the same data, but using the vertical components of the whole ARCES array, confirms this result by measuring  $225.4^\circ$  for the BAZ and 4.3 km/s for the apparent

velocity. After rotation, the L-component shows clearly time-varying amplitudes which cannot be explained as a single S-type polarized onset. Choosing another time window for the 3C analysis may result in different, eventually even totally wrong results, depending on the scattered energy on the Z-component.

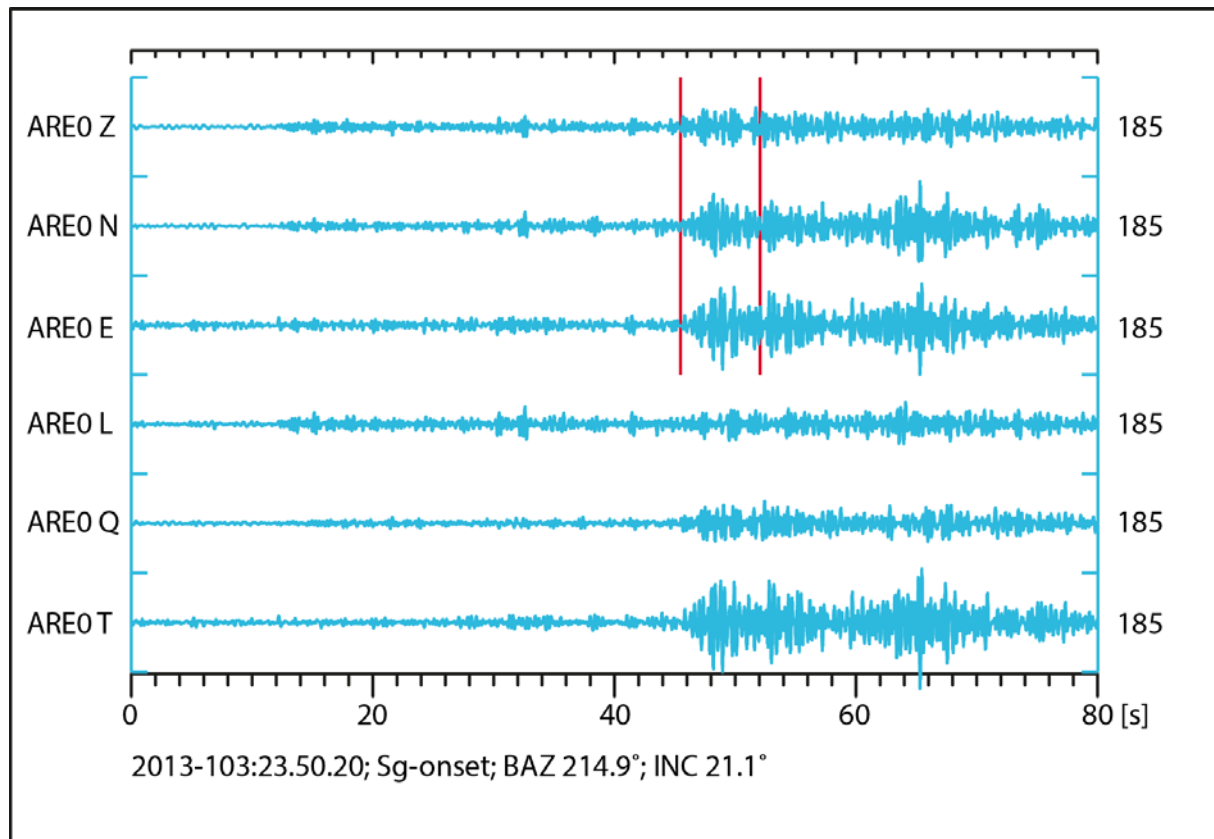


Fig. 6.2.2 Data (bandpass filtered 1.5 – 4 Hz) of a regional Sg-onset observed at the ARCES 3C-site AREO. The time window used for the 3C analysis is marked (red lines) and the maximum amplitude is given on the right. The three top traces show the original 3C (ZNE) and the three bottom traces the LQT-rotated data. For further details see text.

Fig. 6.2.3 shows an icequake recorded very near to the center element SPA0 of the SPITS array on Svalbard (epicentral distance  $\sim 10$  km), here bandpass filtered between 1.5 and 4 Hz. The 3C analysis of the P-onset (red lines) gives a BAZ of  $121.9^\circ$ , which is confirmed by an fk-analysis applied for the full array (BAZ =  $122.6^\circ$ ). The INC value of  $27.8^\circ$  results in an apparent velocity of 12.5 km/s, which is quite high with respect to the fk-result of 4.7 km/s. However, the 3C result for the apparent velocity was calculated using some standard values for P- and S-velocities without taking in account the local velocity structure. The duration of the event is quite short; the S-onset is arriving only 2 s after the P-onset. Already the original Z-component shows that there is significant P-energy arriving during the S-phase. This is mostly a continuation of the P-phase and its coda, but also the effect of the elliptical polarization of SV-energy due to interaction with the free surface. Therefore, it is no surprise that a 3C analysis fails when analyzing a short time window like the one indicated with the dashed magenta lines around the largest S-onset. When using a longer time window (green lines) and analyzing the whole S-phase group one gets BAZ =  $116.9$  and INC =  $64.6$ , which corresponds to an apparent velocity of 3.3 km/s. The full array fk-analysis for the same time window gives BAZ =  $123.5^\circ$  and an apparent

velocity of 2.3 km/s. That the apparent velocity result for the 3C analysis is different from the fk-result can be explained again with the incorrectly modeled local velocity structure.

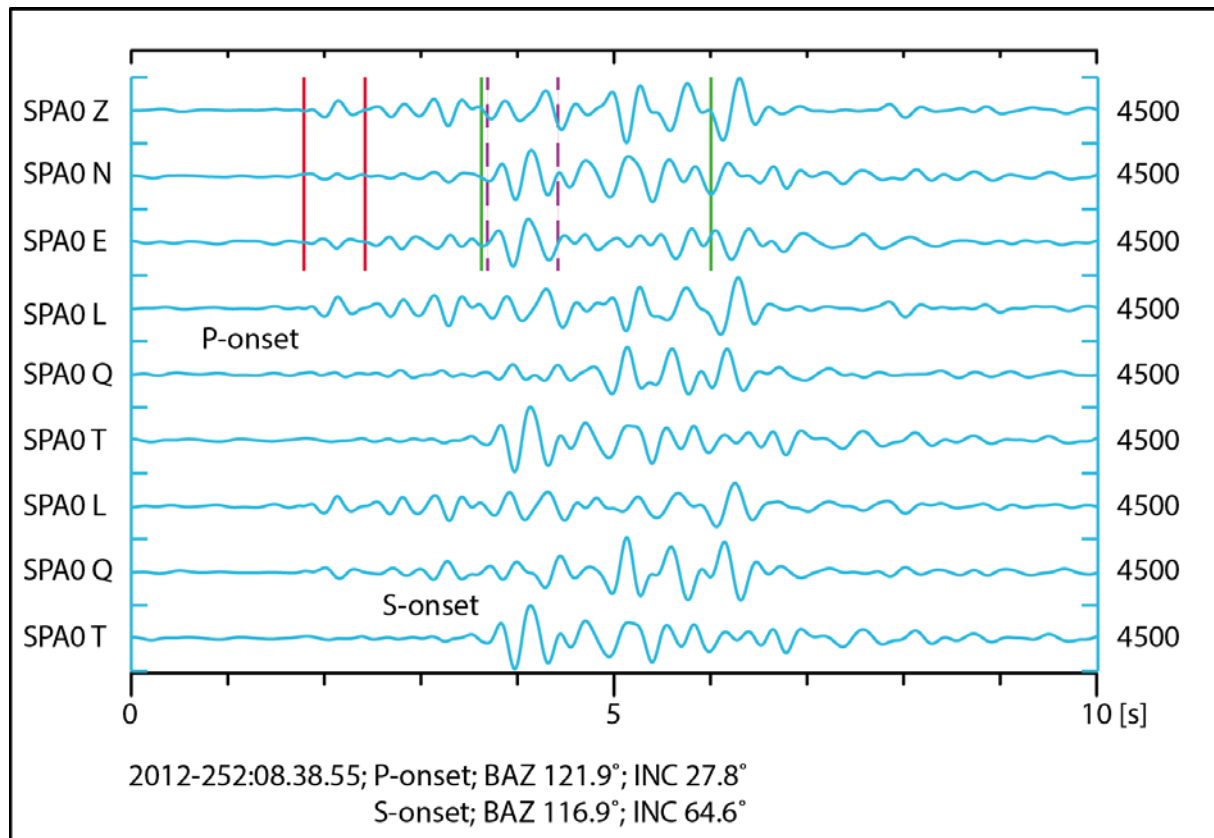


Fig. 6.2.3 Data (bandpass filtered 1.5 – 4 Hz) of an icequake observed at the SPITS 3C-site SPA0. The time window used for the 3C analysis of the P-onset is marked with red lines, of the S-onset with green lines and the amplitude is given on the right. The dashed magenta lines indicate another possible time window to analyze the S-onset. The three top traces show the original 3C (ZNE), the three middle traces the LQT, resulting from rotation using the P-phase parameters, and the three bottom traces the LQT data, resulting from rotation using the S-phase parameters. For further details see text.

Fig. 6.2.4 shows the same icequake as Fig. 6.2.3, but now bandpass filtered between 0.8 and 2.5 Hz. The figure shows a clear Rg-onset on the Z-component, which is typical for events with hypocenters close to the Earth's surface, as e.g., also for icequakes on Svalbard. The figure shows also that the Rg-onset is not so clearly visible on the original horizontal N- and E-components due to still arriving energy of the S-phase and its coda. Here, the correct position and the length of the data window to be analyzed are as critical as in the case of the S-onset. The 3C-analysis of the marked time window correctly identifies the onset as an Rg-onset and finds a BAZ of 121.7°, which is very close to the value achieved by an fk-analysis of all data from the whole array (BAZ 128.25°, apparent velocity 1.63 km/s). The 3C-analysis cannot measure the apparent velocity of a surface wave (here Rg). After rotating the N- and E-components into R- and T-components, the Rg-onset becomes visible on the R-component. The T-component is dominated by S-energy, which already had the largest S-amplitudes after rotating in the LQT-system with S-onset parameters (compare with Fig. 6.2.3). As typical for Rg onsets, a time shift of about  $\frac{1}{4}$  of the dominating signal period is observed between the phase onset on the Z- and the R-component (see the green arrows).

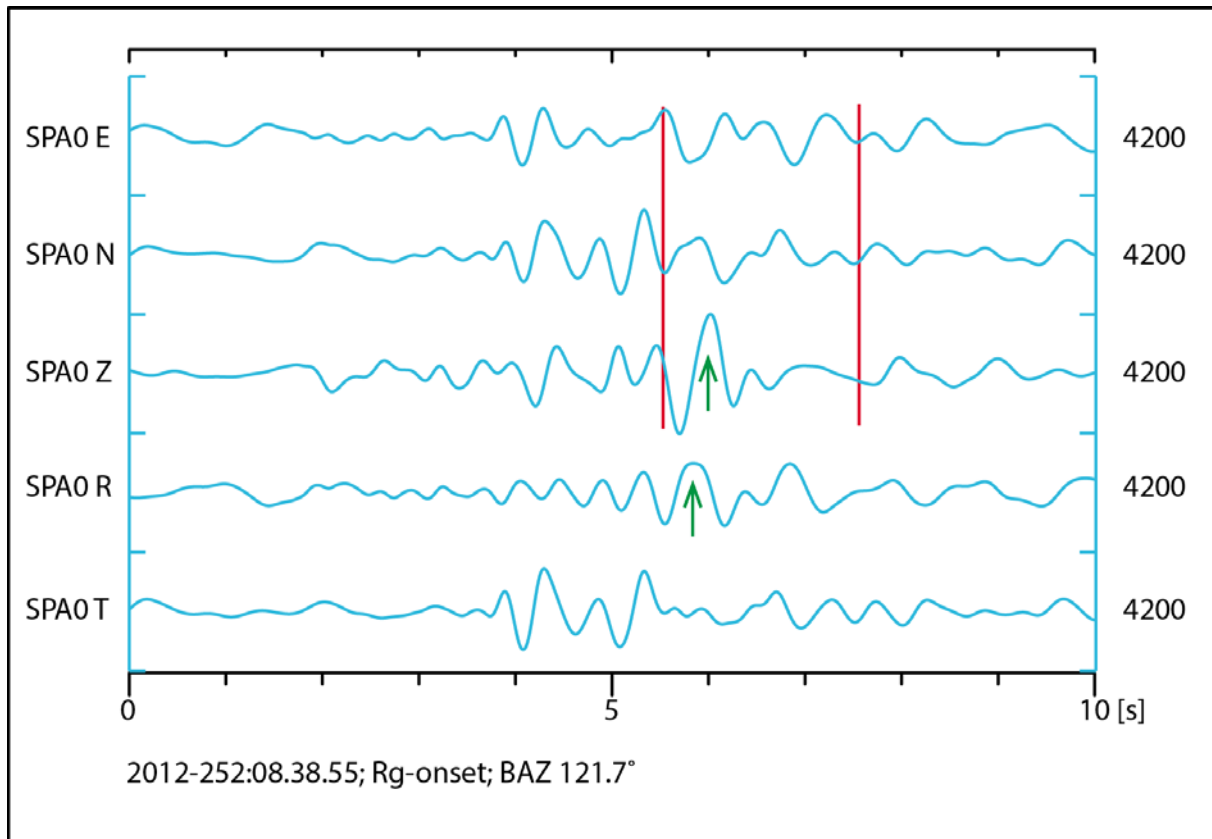


Fig. 6.2.4 As Fig. 6.2.3. The data are now filtered between 0.8 and 2.5 Hz and the red lines show the time window used for the 3C-analysis of the Rg-onset. The three time series on top show the original 3C (ZNE) traces and the two on bottom the R- and T-traces after rotation with the BAZ of the Rg onset. For further details see text.

## 6.2.9 Conclusions

An algorithm to analyze 3C data for phase type, BAZ and INC has been developed, which works fine for ideal data. Reliable results can be achieved also in the case of more noisy and difficult data, as presented in the examples discussed above. However, a systematic study of a large amount of 3C data is missing. For this it is planned to use data from one of NORSAR's arrays and analyze data from array sites with 3C recordings with the tool presented herein. In parallel, a conventional fk-analysis for data from the whole array will be performed as reference. As already seen from the examples shown above, the SNR of the onsets on the different 3C recordings will be particularly critical for the results and it will be interesting to find the SNR-threshold and/or other limits for reliable results from an automated 3C-analysis tool.

J. Schweitzer

**References**

- Müller, G. (2007). Theory of elastic waves. GeoForschungsZentrum Potsdam, Scientific Technical Report STR 07/03, DOI: 10.2312/GFZ.b103-0737, p. 81-84.
- Schweitzer, J., J. Fyen, S. Mykkeltveit, S. J. Gibbons, M. Pirli, D. Kühn and T. Kværna (2012). Seismic Arrays. In: P. Bormann (ed.) (2012), New Manual of Seismological Observatory Practice (NMSOP-2). 2nd (revised) edition, Potsdam: Deutsches GeoForschungsZentrum GFZ., <http://ebooks.gfz-potsdam.de/pubman/item/escidoc:43213:7>; doi:10.2312/GFZ.NMSOP-2\_ch9; 80 pp.
- Wiechert, E. (1907). Über Erdbebenwellen. Theoretisches über die Ausbreitung der Erdbebenwellen. Nachrichten von der Königlichen Gesellschaft der Wissenschaften zu Göttingen, Mathematisch-physikalische Klasse, 413-529.